Preparation of the NaTaO3 Crystal from the KTaO3 Substrate via Topotactic Alkaline Cation Substitution as Confirmed by Transmission Electron Microscopy

Kitta, Mitsunori

Onishi, Hiroshi

eJSSNT Regular Paper

e-Journal of Surface Science and Nanotechnology **18**, 32−37 (2020)

Preparation of the $NaTaO_3$ Crystal from the $KTaO_3$ Substrate via Topotactic Alkaline Cation Substitution as Confirmed by Transmission Electron Microscopy

Mitsunori Kitta,[a, †] Hiroshi Onishi [b]

[a] *Research Institute of Electrochemical Energy, Department of Energy and Environment, National Institute of Advanced Industrial Science and Technology (AIST), 1-8-31, Midorigaoka, Ikeda, Osaka 563-8577, Japan*
[b] *Department of Chemistry, School of Science, Kobe University, Nada, Kobe, Hyogo 657-8501 Japan*
[†] *Corresponding author: m-kitta@aist.go.jp*

Received: 2 December, 2019; Accepted: 12 February, 2020; Published: 22 February, 2020

Orthorhombic-type sodium tantalite ($NaTaO_3$) is one of the most promising photocatalyst for hydrogen generation via water splitting reaction with ultraviolet-irradiation. In this research, we prepared $NaTaO_3$ crystal from $KTaO_3$ substrate via solid-state K^+–Na^+ alkaline cation substitution. In the transmission electron microscopy (TEM) observation revealed the perovskite-type $KTaO_3$ crystal phase is transformed into the orthorhombic crystal phase via simple heating of $KTaO_3$ substrate with Na_2O_2. Atomic scale scanning TEM imaging with energy dispersive X-ray spectroscopy (EDS) are supported that this phase transformation clearly based on the topotactic alkaline cation substitution with K^+ and Na^+ at a common Ta-O basic lattice structure.

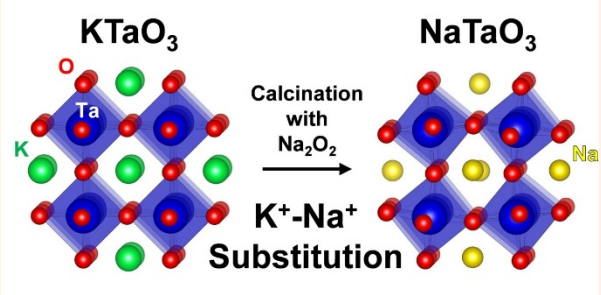

Keywords *Water-splitting photocatalyst; $NaTaO_3$ crystal preparation; $KTaO_3$ single crystal; Topotactic K^+–Na^+ alkaline cation substitution*

I. INTRODUCTION

Recently, a reliable hydrogen-generation reaction is widely promising to the realization of the sustainable energy society. Photocatalytic hydrogen generation is one of the most interested phenomena because of the usage of only water and the solar energy. In order to enhance the photocatalytic activity for the hydrogen-generation reaction, many kinds of metal-oxide based photocatalysts were developed [1]. Among them, orthorhombic-type sodium tantalite ($NaTaO_3$) is a most promising one, since it has many advantages such as a high photocatalytic efficiency under ultraviolet (UV)-light irradiation and an overall water splitting reaction without any sacrificial redox reagents [2−5]. $NaTaO_3$ has been studied as a kind of the $ATaO_3$ (A = Li, Na, K) systems in 1998, which reported that the pure phase of $NaTaO_3$ has relatively weak activity among the $ATaO_3$ system [2]. However, it was revealed later that NiO loading and an excess alkaline preparation enhance greatly the photocatalytic activity of $NaTaO_3$ [5]. The effects of co-catalyst deposition and the excess alkaline preparation were explained as increasing number of the active sites on the $NaTaO_3$ surface. Simultaneously, doping of impurity elements to enhance the photocatalytic activity was studied [5], and it was reported that La-doped $NaTaO_3$ deposited with NiO co-catalyst (NiO/$NaTaO_3$:La) showed greater photocatalytic activity with over 50% of the quantum yield under the UV-light irradiation [5]. The doping effect of La is explained as an alternation of the particle and surface morphology of the $NaTaO_3$ crystals, and a nanoscale step generation on the La-doped crystal surface would contribute to increasing the surface active site. On the other hand, doping of impurities provided other effects to the bulk crystal itself. It generates the active site in the crystal lattice and affects the recombination of photogenerated electrons and holes, as revealed by preceding studies of Sr doping [6,

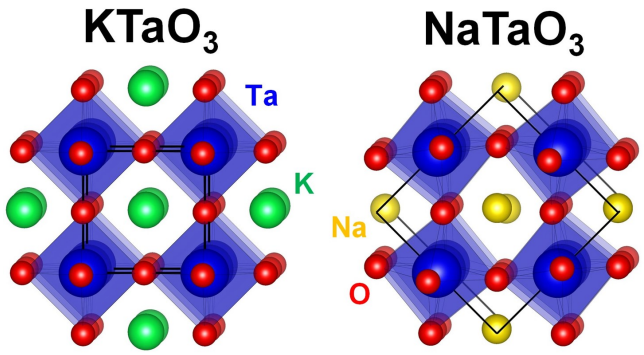

Figure 1: Crystal structure of $KTaO_3$ and $NaTaO_3$. These models were viewed from ⟨001⟩ direction (slightly inclined). K, Na, Ta, and O are shown in green, yellow, blue, and red spheres, respectively. The unit cell of each lattice is shown in black solid lines.

7].

As above, investigations of the bulk crystal and its surface are significantly important to study the photocatalytic mechanism of $NaTaO_3$. However, usual catalysis studies have been performed with $NaTaO_3$ powder samples, and it prevented the fine bulk and surface characterization. In order to approach and reveal the basic mechanism of bulk and surface reactions of the $NaTaO_3$ material, film and substrate preparations by the hydrothermal reaction [8–11], the sol-gel synthesis [12, 13], the flux synthesis [14, 15], and any other deposition methods [16–19] have been studied. However, prepared films by these methods were consisted to be polycrystalline $NaTaO_3$ crystals with complex orientation so that it was not suitable for detailed investigations of the bulk and surfaces of $NaTaO_3$. In the flax-coating methods [15, 20], a hetero-epitaxial growth of well (001)-oriented cubic $NaTaO_3$ crystals was confirmed on the perovskite $SrTiO_3$(001) surface. A selection of the substrate is a key of the well-oriented $NaTaO_3$ crystal growth. The $SrTiO_3$(001) crystal is a suitable substrate for the hetero-epitaxial growth because the lattice structure is similar to $NaTaO_3$. Especially, the lattice mismatch between $NaTaO_3$ (3.931 Å for Ta–Ta distance) and $SrTiO_3$ (3.905 Å for Ti–Ti distance) is less than 1%. For another substrate, perovskite-type $KTaO_3$ (3.988 Å for Ta–Ta distance) is also a promising candidate for the $NaTaO_3$ crystal growth because the lattice mismatch is almost 1%. Especially, these crystals have a common basic structure of the Ta-O lattice, while only the alkaline cation is different. Therefore, the $NaTaO_3$ crystal would be possibly prepared by a simple alkaline-cation substitution from the $KTaO_3$ substrate. Preparation of $NaTaO_3$ from $KTaO_3$ should be interesting in respect to the crystalline preparation, since the single crystalline $KTaO_3$ substrate is commercially available. In previous studies, a cation substitution reaction is confirmed in some perovskite-type oxide materials [21, 22]. Patino *et al.* reported a simple Na and Ni substitution in the $NaTaO_3$ lattice and prepared a $Ni_{0.5}TaO_3$ structure with a topo-chemical reaction [21]. In this substitution reaction, the framework of the Ta-O lattice is almost unchanged. As analogous to this system, a K^+–Na^+ alternation in the $KTaO_3$ crystal is expected, but there is no report to confirm this reaction.

In this study, we tried to prepare the $NaTaO_3$ crystal from a commercially available $KTaO_3$ single crystalline substrate via the K^+–Na^+ alkaline-cation substitution. Figure 1 shows two crystal models of cubic perovskite-type $KTaO_3$ ($Pm\bar{3}m$, a = 3.98830 Å) [23], and orthorhombic-type $NaTaO_3$ ($Pbnm$, a = 5.51300 Å, b = 5.49410 Å, c = 7.75080 Å) [24]. The lattice framework of the Ta and O atoms were closely resembled in $KTaO_3$ and $NaTaO_3$ each other. The position of the alkaline atoms in these two crystals was also similar. Therefore, we assumed that the $NaTaO_3$ crystal would be prepared by the simple K^+–Na^+ substitution of the $KTaO_3$ crystal. Here, we tried the alkaline cation substitution via the solid-state reaction, which was carried out by heating the $KTaO_3$ substrate in sodium vapor atmosphere. The atomistic K^+ and Na^+ substitution in the common Ta-O lattice structure was confirmed by a transmission electron microscopy (TEM) study.

II. EXPERIMENTAL

A commercially available $KTaO_3$(001) substrate (purchased from Crystal Base) was cut into the size of 2 mm × 2 mm × 0.2 mm and was thinned by Ar^+ milling systems (PIPS, GATAN) to prepare thin specimen for the TEM study. The thinned $KTaO_3$(001) specimen was calcined with 0.5–1 mg of sodium peroxide (Na_2O_2) granular in air at 1073–1123 K for 15–18 h using 15 mL of an alumina crucible (Al_2O_3, > 99%). After the calcination, the Na_2O_2 granular disappeared in the crucible. It indicated that Na_2O_2 was vaporized and the Na vapor would react with the $KTaO_3$ specimen during the calcination process, as similar to the the Li-vapor source [25]. The calcined thin specimen was characterized by TEM (JEM-3000F, JEOL) at 200 kV with bright field TEM imaging and selected-area electron diffraction (SAED) analysis. The TEM images and diffractgrams were recorded by a slow-scan CCD camera (Orius SC-200, GATAN). The same specimen was also characterized by high angle annular dark field scanning TEM (HAADF-STEM) by high resolution analytical TEM (TITAN^{3TM} 60-300, FEI) with atomistic energy dispersive X-ray analysis (ChemiSTEM^{TM} EDS) [26] performed by the super-X detector and analyzed by the software (Esprit, Bruker).

III. RESULTS AND DISCUSSION

The feature of prepared specimen was confirmed by conventional transmission electron microscopy imaging. Figure 2 shows the low-magnification image of specimens and the corresponding electron diffractograms. As-shaved $KTaO_3$ specimen in the TEM image of Figure 2(a), where the thin-edge of the specimen is curving due to the

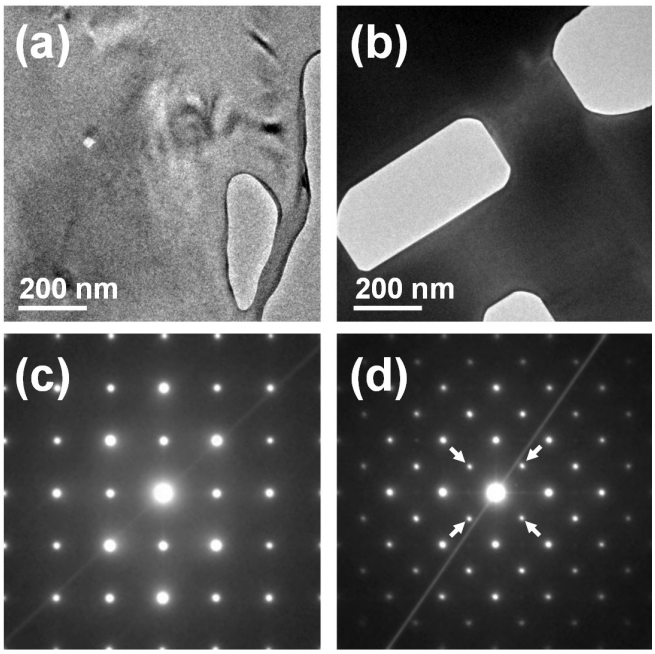

Figure 2: TEM investigation of crystal alternation before and after calcination. Low-magnification TME images of (a) the as-shaved $KTaO_3$ substrate and (b) the calcined specimen. Electron diffraction patterns of (c) the as-shaved $KTaO_3$ substrate and (d) the calcined specimen. Newly generated diffraction spots of the calcined specimen are indicated by arrows in (d).

fabrication damage of Ar^+ milling. On the other hands, the specimen after the calcination with Na_2O_2 shows a typical crystal facets, as show in Figure 2(b). This suggests that the fabrication damage layer of the as-shaved $KTaO_3$ specimen was re-crystallized via the calcination process. Therefore, the morphology of the specimen is slightly altered after the calcination. The electron diffractograms of $KTaO_3$ and the prepared specimen are shown in Figure 2(c, d). Clear diffraction spots are seen for both specimens, whereas the diffraction patterns are quite different from each other. The diffraction pattern of Figure 2(c) corresponds to the $KTaO_3$ lattice with a cubic perovskite-type structure. However, the specimen calcined with Na_2O_2 shows a different character from the $KTaO_3$ lattice, because new extra diffraction spots, indicated by white arrows in Figure 2(d), are clearly observed. These extra diffraction spots were never seen in the cubic perovskite-type structure, and it means that $KTaO_3$ was not re-crystallized as a simple $KTaO_3$ crystal but was transformed into another type of the crystal. The newly generated diffraction spots correspond to the "double diffraction" of the orthorhombic-type $NaTaO_3$ lattice structure, as explained in Figure S1 in Supplementary Material.

The lattice transformation usually affects the lattice strain. Thus, the calcined specimens might have some lattices defects or dislocations. To confirm the crystallinity of the calcined specimen, HAADF-STEM imaging was performed, and the results are shown in Figure 3. A photograph of the prepared specimen is shown in Figure 3(a). Cracks or

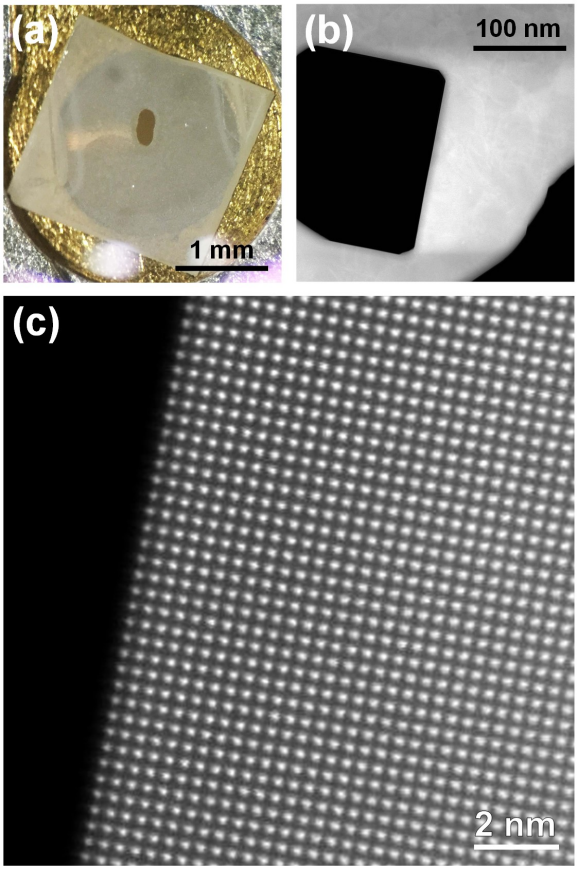

Figure 3: HAADF-STEM imaging of the calcined specimen. (a) Photograph of the prepared specimen's appearance. HAADF images of the prepared specimen acquired with (b) low- and (c) high-magnification atomic-scale resolutions, respectively.

destructions were not seen in the overall of specimen, suggesting that the preparation procedure did not bring considerable damage to the substrate. Low-magnification HAADF image of the specimen [Figure 3(b)] did not show typical crystalline defects or a dislocation contrast. This also suggests a less damage of the specimen. The crystal facet was shapely grown, meaning that the crystallinity of the calcined specimen is remarkably high. An atomic-scale HAADF image of the specimen is presented in Figure 3(c). The bright contrast of the crystalline lattice shows a Ta atomic column, since Ta is the highest *Z*-number element among the Na(K)-Ta-O component. A crystal facet of the specimen was also observed in the atomic scale. At the facet, the Ta atoms were arranged to form an atomically flat surface, as the high-temperature calcination naturally forms a stable crystal surface in a thermodynamic process. In the lattice structure, the neighboring Ta lattice spacing is calculated from the STEM image as 3.9 Å, which corresponds to the Ta−Ta atomic distance in the $NaTaO_3$ and $KTaO_3$ lattices. Further, the lattice dislocation or a strain was also not observed. These results suggest that the basic Ta lattice framework should be stably retained during the crystallization process of the Na_2O_2-calcination.

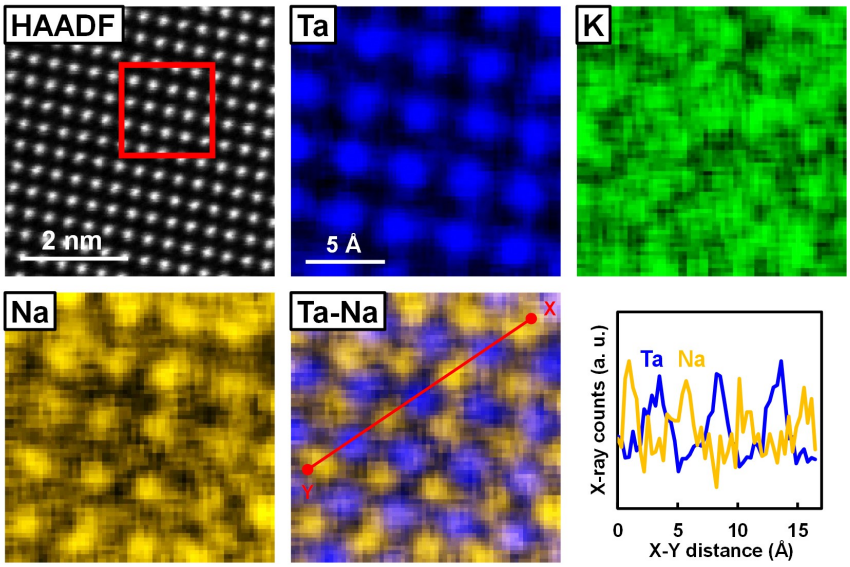

Figure 4: STEM-EDS elemental mapping of the calcined specimen with an atomic scale resolution. EDS mapping was performed at the area of a red square as shown in the HAADF image. Na and Ta elemental intensity profiles are shown along the X−Y line in the Ta−Na overlay image.

As discussed, the crystallization of the $NaTaO_3$ lattice should proceed while the basic Ta-O lattice structure of the $KTaO_3$ crystal is preserved. Namely, the $NaTaO_3$ crystal should be grown via a K^+−Na^+ substitution in the $KTaO_3$ crystal which is a template of the Ta-O lattice structure. To confirm the atomistic substitution of the K^+ and Na^+ alkaline cations, we performed atomic-scale EDS elemental mapping of the calcined specimen. Ta, K, and Na elemental mapping images acquired from a red square area of the HAADF image are presented by blue, green, and yellow colors, respectively (Figure 4). The K mapping image shows no characteristic contrast, while the Na mapping image clearly shows a well-ordering atomic contrast corresponding to the $NaTaO_3$ lattice. This $NaTaO_3$ lattice character is better confirmed in the Ta−Na overlay image. The atomic arrangements of Na and Ta nicely fit the $NaTaO_3$ crystal structure, as shown in Figure 1. The X-ray counts of each atomic site were evaluated along the X−Y line in the Ta−Na overlay image. The elemental intensity corrugation was clearly confirmed, suggesting that Na^+ substitutes exactly for K^+ in $KTaO_3$. It should be noted that the X-ray counts of K^+ was not confirmed in the site selected EDS spectra of this mapping image at least within the detection sensitivity of EDS analysis, as shown in Figure 5. It is worth mentioning that the substitution of K^+ for Na^+ proceeds well. In the calcination process, the vaporized Na-salt would react with the thin edge of the $KTaO_3$ crystal, and Na^+ would insert into the K^+ site. Insertion of Na^+ in $KTaO_3$ would not favor a solid-solution-like lattice structure because of a considerable difference in the cationic radii (r_{K^+} = 138 pm and r_{Na^+} = 102 pm) so that the solid-solution-like lattice would not be energetically stable. Therefore, Na^+ insertion leads to pushing out of K^+ from the $KTaO_3$ lattice and crystallizing into the $NaTaO_3$ lattice. Of course, purged K^+

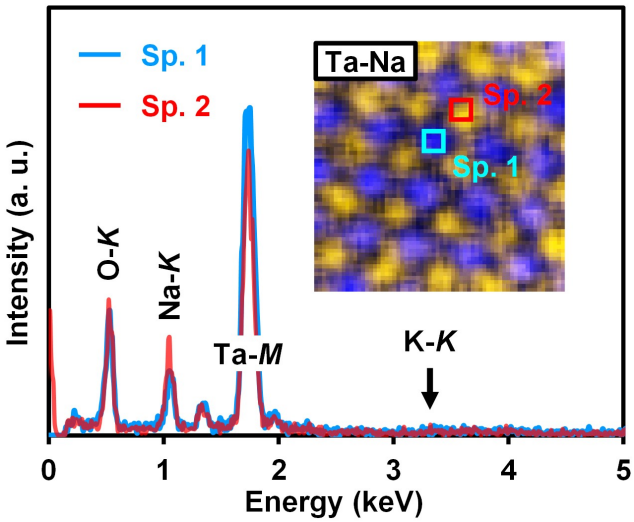

Figure 5: EDS spectra extracted from Ta (Sp. 1) and Na (Sp. 2) atomic column positions. Blue and red lines of the spectra correspond to the blue and red square areas in the Ta−Na overlay image, respectively. The K-*K* X-ray line at 3.3 keV was not confirmed in both spectra.

was concentrated in other parts of the area in the specimens. This was confirmed by low-magnification EDS mapping, as presented in Figure 6. K elemental mapping shows K-rich and poor domains, and the K-poor domains should be generated by the Na^+ substitution. The elemental mapping of the Na and K overlay image well indicates the opposite distribution characters of each element. The EDS spectra extracted from the K-poor (Sp. 1) and rich (Sp. 2) regions also show this character. The K-*K* X-ray intensity is scarcely observed at the K-poor region, suggesting that the Na insertion into the $KTaO_3$ lattice should remove considerably

the K cations. Contrastingly, the Na-*K* EDS signal was observed even at the K-rich region. Therefore, Na should exist there and would be inserted in the K atomic site. The atomic scale EDS mapping acquired from the K-rich region is shown in Figure 7. The elemental mapping images corresponding to the red square area shown in the HAADF image were presented at the same colors as those in Figure 4. Na and K elemental mapping images show a clear contrast at the same atomic column positions. The K-*K* (green) and Na-*K* (yellow) X-ray intensity line profiles are shown along to the X−Y line presenting in the K−Na overlay image. The intensity profiles of the K and Na elements correspond well to each other, strongly supporting that the K^+–Na^+ substitution should really occur at the same atomic-site of a common Ta-O lattice between $KTaO_3$ and $NaTaO_3$ with a topotactic manner.

As above results, a completely pure $NaTaO_3$ crystal may be difficult to prepare. However, we insist that the simple K^+–Na^+ substitution is realized in the $KTaO_3$ lattice. A commercially available $KTaO_3$ substrate will be a better material and the well-defined crystalized $NaTaO_3$ specimen will be prepared from a $KTaO_3$ single crystal.

IV. CONCLUSIONS

A $NaTaO_3$ crystal was prepared from a commercially available $KTaO_3$ substrate via simple calcination with Na_2O_2. In the calcination process, Na_2O_2 vaporized and reacted with the $KTaO_3$ crystal. The crystal structure of the cubic perovskite-type $KTaO_3$ lattice transformed into the orthorhombic-type $NaTaO_3$ lattice after the calcination, as confirmed by electron diffractogram. HAADF-STEM imaging revealed that the calcined specimen retained a Ta atomic periodicity of the $KTaO_3$ crystal without any dislocation or defect. Atomistic EDS mapping clearly shows

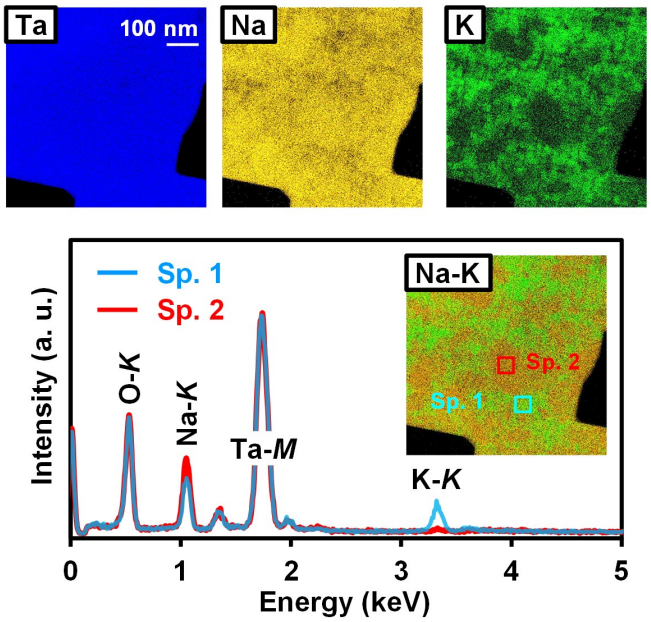

Figure 6: EDS elemental mapping with a low-magnification scale (upper). EDS spectra from K-rich (Sp. 1) and poor (Sp. 2) regions indicated by blue and red squares in the Na and K overlay image are shown by the corresponding colors (lower). The K-*K* X-ray signal intensity is observed in the K-rich region, whereas the Na-*K* signal intensity is opposite to that.

that Na^+ substitutes for K^+ in the $KTaO_3$ lattice and the $NaTaO_3$ crystal is grown. The atomistic substitution would be caused by the difference in the ionic radius of the Na^+ and K^+ cations, and ionic separation should be energetically more favorable than the solid-solution-like phase formation. The $NaTaO_3$ crystal lattice could be prepared by the simple K^+–Na^+ substitution in the $KTaO_3$ crystal, meaning that a well-defined high-crystalline $NaTaO_3$ specimen will be

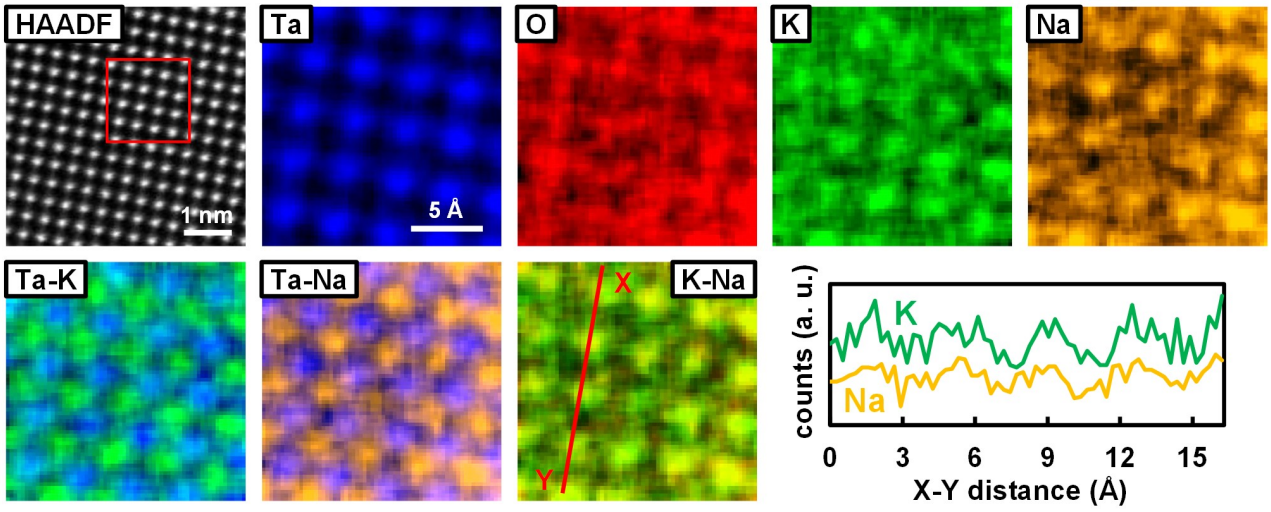

Figure 7: Atomistic EDS mapping acquired from the K-rich region showing in Figure 6. The EDS mapping was performed in the area of a red square in the HAADF image. Elemental intensity line profiles are analyzed along to the X−Y line presenting in the K−Na overlay image. The K-*K* and Na-*K* intensity profiles exhibit a similar corrugation, indicating that these elements substituted at the same site of the basic Ta-O lattice structure.

acquired from a commercially available $KTaO_3$ single crystal substrate.

Acknowledgments

This work was supported by JSPS KAKENHI Grant Number 18KK0161.

Appendix

A detailed explanation of the double diffraction of the $NaTaO_3$ crystal is available in Supplementary Material at https://doi.org/10.1380/ejssnt.2020.32.

References

[1] A. Kudo and Y. Miseki, Chem. Soc. Rev. **38**, 253 (2009).
[2] H. Kato and A. Kudo, Chem. Phys. Lett. **295**, 487 (1998).
[3] H. Kato and A. Kudo, Catal. Lett. **58**, 153 (1999).
[4] H. Kato and A. Kudo, J. Phys. Chem. B **105**, 4285 (2001).
[5] H. Kato, K. Asakura, and A. Kudo, J. Am. Chem. Soc. **125**, 3082 (2003).
[6] M. Maruyama, A. Iwase, H. Kato, A. Kudo, and H. Onishi, J. Phys. Chem. C **113**, 13918 (2009).
[7] L. An and H. Onishi, ACS Catal. **5**, 3196 (2015).
[8] Y. Lee, T. Watanabe, T. Takata, J. N. Kondo, M. Hara, M. Yoshimura, and K. Domen, Chem. Mater. **17**, 2422 (2005).
[9] X. Zhou, Y. Chen, H. Mei, Z. Hu, and Y. Fan, Appl. Surf. Sci. **255**, 2803 (2008).
[10] M. Zhang, G. Liu, D. Zhang, Y. Chen, S. Wen, and S. Ruan, J. Alloys Compd. **602**, 322 (2014).
[11] L. Polak, T. P. N. Veeken, J. Houtkamp, M. J. Slaman, S. M. Kars, J. H. Rector, and R. J. Wijingaarden, Thin Solid Films **603**, 413 (2016).
[12] Š. Kunej, A. Veber, and D. Suvorov, J. Am. Ceram. Soc. **96**, 442 (2013).
[13] Y. Lee, T. Watanabe, T. Takata, J. N. Kondo, M. Hara, M. Yoshimura, and K. Domen, Chem. Mater. **17**, 2422 (2005).
[14] S. Suzuki, K. Teshima, S. Maruyama, Y. Matsumoto, K. Domen, and S. Oishi, CrystEngComm **15**, 4058 (2013).
[15] S. Suzuki, H. Wagata, K. Yubuta, S. Oishi, and K. Teshima, CrystEngComm **17**, 9016 (2015).
[16] F. Schlottig, J. Schreckenbach, and G. Marx, Fresenius J. Anal. Chem. **363**, 209 (1999).
[17] C. Reitz, K. Brezesinski, J. Haetge, J. Perlich, and T. Brezesinski, RSC Adv. **2**, 5130 (2012).
[18] S. Suzuki, K. Teshima, K. Yubuta, S. Ito, Y. Moriya, T. Takata, T. Shishido, K. Domen, and S. Oishi, CrystEngComm **14**, 7178 (2012).
[19] A. M. Huerta-Flores, J. Chen, L. M. Torres-Martínez, A. Ito, E. Moctezuma, and T. Goto, Fuel **197**, 174 (2017).
[20] T. Fujiwara, L. An, Y. Park, N. Happo, K. Hayashi, and H. Onishi, Thin Solid Films **658**, 66 (2018).
[21] M. A. Patino, T. Smith, W. Zhang, P. S. Halasyamani, and M. A. Hayward, Inorg. Chem. **53**, 8020 (2014).
[22] S. Joo, O. Kwon, K. Kim, S. Kim, H. Kim, J. Shin, H. Y. Jeong, S. Sengodan, J. W. Han, and G. Kim, Nat. Commun. **10**, 697 (2019).
[23] E. A. Zhurova, V. E. Zavodnik, and V. G. Tsirel'Son, Crystallogr. Rep. **40**, 753 (1995).
[24] M. Ahtee and L. Unonius, Acta Cryst. A **33**, 150 (1977).
[25] M. Kitta, T. Akita, Y. Maeda, S. Tanaka, and M. Kohyama, Surf. Interface Anal. **46**, 1245 (2014).
[26] Application Note; *ChemiSTEM™ Technology A revolution in EDX analytics* (FEI Company), available at http://photos.labwrench.com/equipmentManuals/11006-4390.pdf (Last accessed on 27 December, 2019).